Highly Luminescent Colloidal Nanoplates of Perovskite Cesium Lead Halide and Their Oriented Assemblies

Yehonadav Bekenstein[†§], Brent A. Koscher[†§], Samuel W. Eaton[†], Peidong Yang[†‡§∥], and A. Paul Alivisatos[*†‡§∥]

[†] Department of Chemistry, University of California, Berkeley, California 94720, United States

[‡] Department of Materials Science and Engineering, University of California, Berkeley, California 94720, United States

[§] Materials Sciences Division, Lawrence Berkeley National Laboratory, Berkeley, California 94720, United States

[∥] Kavli Energy NanoScience Institute, Berkeley, California 94720, United States

J. Am. Chem. Soc., **2015**, *137* (51), pp 16008–16011

DOI: 10.1021/jacs.5b11199

Publication Date (Web): December 15, 2015

*ap_alivisatos@berkeley.edu

•

Abstract

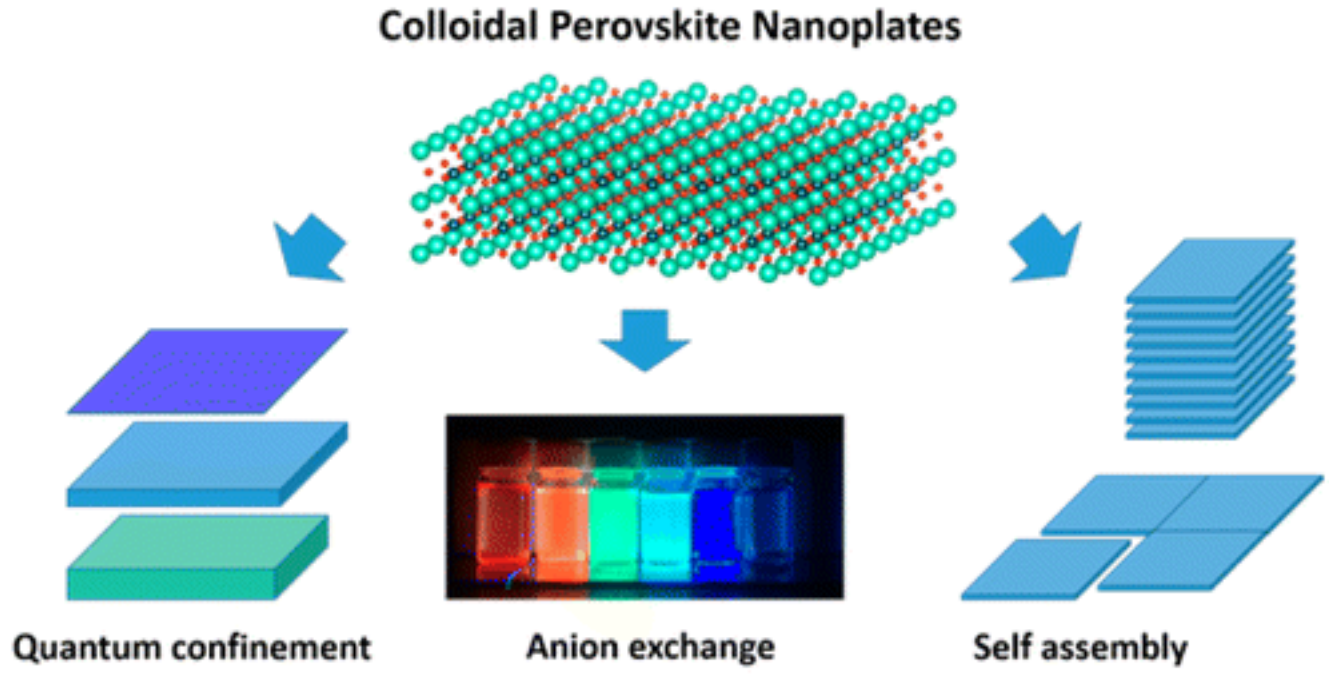

Anisotropic colloidal quasi-two-dimensional nanoplates (NPLs) hold

great promise as functional materials due to their combination of low dimensional optoelectronic properties and versatility through colloidal synthesis. Recently, lead-halide perovskites have emerged as important optoelectronic materials with excellent efficiencies in photovoltaic and light-emitting applications. Here we report the synthesis of quantum confined all inorganic cesium lead halide nanoplates in the perovskite crystal structure that are also highly luminescent (PLQY 84%). The controllable self-assembly of nanoplates either into stacked columnar phases or crystallographic-oriented thin-sheet structures is demonstrated. The broad accessible emission range, high native quantum yields, and ease of self-assembly make perovskite NPLs an ideal platform for fundamental optoelectronic studies and the investigation of future devices.

Freestanding quasi-two-dimensional (2D) nanoplates (NPLs) have demonstrated exceptional photophysical properties, such as increased exciton binding energy, enhanced absorption cross sections with respect to bulk, low threshold stimulated emission, and notable optical nonlinearities.(1a-1c) Established colloidal synthetic methods enable exquisite control of their thickness and hence also optical properties. Moreover, controlling ligand interactions provides a route for the self-assembly of the NPLs into more complex structures.(2a, 2b) These characteristics highlight colloidal NPLs as an interesting class of nanocrystal geometry for future photophysical studies. Recently, metal halides with the perovskite crystal structure have emerged as important optoelectronic materials. The combination of excellent optical and electronic properties have already been used to demonstrate remarkable conversion efficiencies in photovoltaics and light emitting diode devices.(3a, 3b) These layered materials exhibit an ABX_3 crystal structure, where A is a monovalent cation and B is an inorganic–metal cation in an octahedral coordination with six halide ions, X. Recent studies have concentrated on thin film perovskite with A being an organic cation typically methylammonium. Nanocrystals of these organic–inorganic hybrid perovskite were synthesized with control over their shape, forming 2D materials and colloidal quasi-2D NPLs presenting quantum size effects.(4a-4c) As material stability is currently limiting the application of hybrid-based devices, all-inorganic perovskites, in which cesium replaces the organic cation, may yield improved

stability in comparison to hybrid perovskites, as well as extending the range of materials, which can be investigated.(5)
Recently a synthetic protocol for three dimensionally confined all-inorganic colloidal cesium lead-halide perovskite nanocrystals was reported.(6a-6c) The resulting nanocubes present excellent photoluminescent quantum yields (PLQYs) of up to ~90% without requiring additional surface passivation. This exciting result motivated us to synthesize colloidal nanocrystals with quasi-2D geometries.
We report the colloidal synthesis of lower symmetry all-inorganic cesium lead halide perovskite nanoplates and demonstrate their assembly to either form stacked columnar structures or to fuse into thin oriented sheets. We directly synthesize perovskite $CsPbBr_3$ NPLs, and through anion exchange, we readily control the halide composition forming $CsPbI_3$, $CsPbCl_3$, and mixed compositions with band gap emission covering the entire visible spectrum (385–690 nm). Due to the high PLQYs of ~80% and ability to self-assembly into higher ordered structures, all-inorganic perovskites NPLs are an interesting system for the study of quantum confinement effects and are positioned to be favorable candidates for future devices, combining the excellent optoelectronic properties of perovskites with 2D geometry.
Colloidal synthesis of $CsPbBr_3$ perovskite NPLs was carried out by modifying the nanocrystal synthesis reported by Protesescu et al.(6a) in which they demonstrated size control of nanometer sized cubes by varying the temperature from 140 to 200 °C. We have discovered that reactions at lower temperatures between 90 and 130 °C tend to strongly favor asymmetric growth producing quasi 2D geometries. NPLs were synthesized using standard air-free techniques. $PbBr_2$ was solubilized in octadecene (ODE) with oleic acid and oleylamine, and then Cs-oleate was injected at elevated temperatures (90–130 °C) to form NPLs.

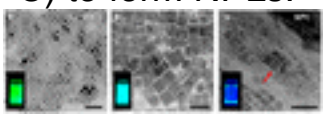

Figure 1. Study of the influence of reaction temperature in $CsPbBr_3$ colloidal synthesis. (a) At 150 °C, green emitting 8–10 nm nanocubes are formed. (b) At 130 °C, cyan emitting nanoplates with lateral dimensions of

20 nm and thickness of a few unit cells (~3 nm) are formed. (c) At 90 °C, blue emitting thin nanoplates are observed, along with several-hundred nanometers lamellar structures. We observe NPL growth along the lamellae (red arrow) (a–c, scale bar is 50 nm).

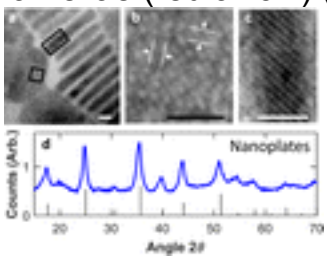

Figure 2. (a) HR-TEM micrograph depicting atomic resolution of both flat lying and stacked NPLs. Two areas of interest are blown up. (b) Top view of the NPL depicting *d* spacing of ~0.58 nm typical for cubic phase $CsPbBr_3$. (c) Side-view of stacked NPLs with typical thickness of ~3 nm corresponding to five perovskite unit cells (a–c scale bar 3 nm). (d) XRD spectra of cubic phase $CsPbBr_3$ NPLs compared to the standard powder diffraction pattern of cubic bulk $CsPbBr_3$ ($\lambda_{Co\text{-}k\alpha}$ = 1.79 Å).

The ionic nature of the metathesis reaction dictates the rapid nucleation and growth kinetics of the resulting nanocrystals. We observed that the reaction temperature plays a critical role in determining the shape and thickness of the resulting NPLs. Reactions conducted at 150 °C produce mostly symmetrical nanocubes with green-color PL emission (Figures 1a).(6a-6c) Reactions conducted at lower temperatures present blue-shifted PL spectra, for example, at 130 °C lower symmetry NPLs with cyan emission are formed (Figures 1b and S1). At 90 and 100 °C, very thin NPLs were detected along with lamellar structures ranging 200–300 nm in length. As TEM images depict, NPLs grow along and inside these lamellar structures (Figures 1c and S2), suggesting that organic mesostructures serve as growth directing soft templates that break the crystal's inherent cubic symmetry and dictate the 2D growth. Such a mechanism is not without precedent, where a similar soft templating mechanism was reported for wurtzite CdSe NPLs.(7) Reaction temperatures as low as 70 °C resulted in almost transparent suspensions, where the TEM showed amorphous micron size sheets with almost no crystals present, from this we hypothesize these objects are unreacted precursors (SI Figure S3). Interestingly, reactions at temperatures of 170–200 °C produce bigger NCs and at longer reactions times high

aspect ratio nanowires (SI Figure S4). Recent reports suggest these geometries evolve sequentially from each other.(8)
To characterize the NPL structure the crude reaction suspension was centrifuged and cleaned. Cleaning the perovskite NPLs has been a challenging task, primarily due to the ionic nature of these crystals and their sensitivity to water, which makes them susceptible to degradation. NPLs are precipitated from ODE by centrifugation. However, after redispersion of the NPLs in hexane or toluene, any additional cleaning and separations are nontrivial, as typical methanol/acetone washing techniques dramatically reduce the bright PL and physically degrade the NPLs as verified by TEM (SI Figure S5). We have carefully tested a library of antisolvents that would destabilize the colloidal suspension without reducing their PLQY. We observed that ethyl acetate and methyl–ethyl ketone with polarity indexes of 4.4 and 4.7, respectively,(9) are sufficiently polar to initiate NPL aggregation and precipitation upon centrifugation on the one hand, but prevent degradation and maintain the high PLQY on the other. This may be directly related to the low water solubility of these solvents (8.7% and 24%, respectively) and therefore also low inherent water content. Previous studies have shown that water dramatically degrades and reduces the PL efficiency of perovskite-based devices.(10) We have observed a similar effect, of reduced PLQYs from the NPLs upon exposure to liquid water. The cleaned NPL suspension was further characterized by TEM and XRD. The NPLs present a lateral square geometry with a thin third dimension. The NPLs display a tendency to form stacked assemblies on their sides, allowing facile direct measurement of the NPL thickness with atomic resolution. Typically reactions at 130 °C yield a majority of NPLs with lateral dimensions of ~20 nm and thickness of ~3 nm, which correspond to five unit cells (Figure 2a,c). These agree with thickness measured using small-angle X-ray scattering (SAXS discussed later). *d*-spacing values of 0.58 nm are measured (Figure 2b) in agreement with reported values of cubic $CsPbBr_3$ unit cells.(11) Materials of $CsPbX_3$ are known to exist in a variety of crystal phases, including orthorhombic, tetragonal, and cubic crystal phases. Of these, the cubic phase is the energetically stable crystallographic phase at elevated temperatures for all compounds.(11) Remarkably,

in the case of $CsPbBr_3$ NPLs the high temperature cubic phase remains stable even at room temperature (Figure 2d). Likewise, $CsPbBr_3$ nanocubes maintain a stable room temperature cubic crystallographic phase(6a) (SI Figure S6). Interestingly, $CsPbBr_3$ micron size nanowires, although 12 nm in diameter, exhibit the orthorhombic phase.(8) The two phases present markedly different optical properties, with the cubic phase being highly luminescent with PLQYs of 80–90% and the orthorhombic phase having significantly lower PLQYs.

Absorption and PL spectra are presented in Figure 3a. The absorption spectrum is dominated by sharp exciton peaks; similar features were previously reported for CdSe NPLs,(1b) and recently also in hybrid perovskite NPLs.(4a, 4b) Reactions at lower temperatures present a blue-shift of the absorption and emission peaks and in some cases very small Stokes shifts (~30 meV). The PL emission shifts from green (512 nm 2.5 eV) to deep purple (405 nm 3 eV) for the strongly quantum confined band edge emission (Figure 3a). A typical reaction produces a mixture of PL peaks at fixed energies. The intensities of these peaks are directly related to the reaction temperature, amount of cleaning, and separations. We hypothesize that these successive emission peaks arise from NPLs with well-defined thickness that differ in thickness by an integer number of perovskite unit cells. Specifically we measured peaks at 488, 477, 462, 435, and 405 nm, where these may be assigned to thicknesses of 5, 4, 3, 2, and 1 Perovskite unit cells, respectively. In the case of the thicker plates, we were able to confirm this assumption by directly measuring the thickness of stacked NPLs with atomic resolution using HRTEM (Figure 2c). The different NPLs populations can be separated by size-selective precipitation. The thinner plates (mono and bilayers) could be easily separated from the other populations, but difficult to separate from each other. Similarly, separation of the three, four, and five layered plates proved to be challenging. However, by selectively exciting the different populations at near band-edge energies, one can separately investigate the different populations (SI Figure S7). High PLQY values of 84.4 ± 1.8%, 44.7 ± 2.6%, and 10 ± 0.5% were measured for the five, four, and three monolayer thick NPLs. These high values are surprising

since one would expect that the plate geometry, with its inherently high surface to volume ratio will be exceptionally sensitive to surface defects and exhibit low PLQY. This effect may indeed be reflected by the somewhat lower PLQY measured for the thinner plates. Traditionally a protective shelling layer of a wider band gap semiconductor is used for this purpose. For example 80% PLQY was possible in CdSe plates only after a protective CdS shell was grown.(12) The high PLQYs are retained also in the other lead-halide compositions. By using a facile anion exchange process in which the Br^- anions are replaced with either Cl^- or I^-, we are able to tune the platelets composition and therefore their emission spectra to cover all of the visible spectrum from typical 488 nm (with 80 meV fwhm) in the Br^- deep red emission of 660 nm (fwhm 120 meV) in the I^- and deep purple emission of 405 nm (fwhm 107 meV) in the Cl^- case (Figure 3b,c). Interestingly, in respect to recent reported anion exchange results,(13a, 13b) the emission peaks of the exchanged NPLs are blue-shifted, consistent with quantum confinement. This along with TEM imaging further confirms that the 2D plate geometry is preserved also after the anion exchange process.

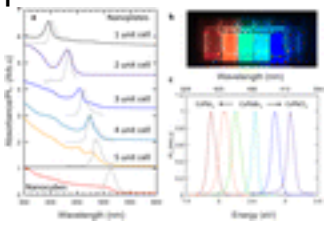

Figure 3. (a) Absorption (solid lines) and emission (dashed lines) spectra of NPLs and nanocubes for comparison. Five different emission peaks at fixed wavelengths can be resolved; these correspond to five different thicknesses of the plates (1–5 unit cells). (b) Colloidal solution of anion exchanged NPLs in hexane under UV illumination (λ = 365 nm) spanning the entire visible spectrum. Corresponding PL spectra of the halide-anion exchanged samples.

The perovskite NPLs show a clear tendency to self-assemble into two different hierarchical structures. The first is assembly into stacked columnar phases, which form in concentrated NPL solutions when ligands strongly interact. These were characterized optically (SI Figure S8) and by TEM and SAXS. For a slowly dried sample, the SAXS intensity is anisotropic and characteristic of stacked plates in the out-of-plane orientation with respect to the substrate (Figure 4a

and inset). In the angular 1D data, peaks at q values of 0.327 and 1.068 nm^{-1} are observed, these correspond to distances of 19.5 and 5.77 nm, which are the NPL lateral dimensions and thickness, respectively. These distances also include the length of the organic ligands; specifically, oleates and oleylammonium, ligands that are known to densely pack on surfaces, have already been reported to support NPL attachment into columnar phases.(1a, 2b) By combining SAXS and TEM data one can calculate the effective distance between the stacked plates as ~2.7 nm, which is smaller than the reported 3.6 nm for an oleate double layer length. This can be explained by the intercalation of the ligand hydrocarbon chains, adding to the structural strength of these assemblies.(1a) Indeed we observe that once formed, stacked NPLs are difficult to breakdown with sonication. Interestingly, the 0.327 nm^{-1} peak presents also higher order peaks at $2q$ (0.654 nm^{-1}) and $3q$ (0.982 nm^{-1}), and these higher harmonics demonstrate the long-range ordering in the samples and are also a consequence of the relatively high electron density of the plates. The second type of assembled structures are large 2D sheets formed by lateral crystallographic oriented attachment of single plates. These assemblies typically form in dilute samples where ligand passivation is destabilized. Weller et al.(1a) have reported a process of directed oriented attachment of PbS NCs into 2D plates with micron-sized lateral dimensions by the addition of alkene-halide cosolvents. Following this work, we have tested the effect of adding various alkene-halides and dialkene-halides to the NPL suspension. This was typically preformed in ODE after which the suspension was heated to 110 °C for 5–15 min (more details in SI). The suspension was cleaned and characterized optically (SI Figure S9), by TEM and AFM. Typically large sheets of perovskite $CsPbBr_3$ of square/rectangular shapes with lateral dimensions of a few hundred nanometers were readily measured following the treatment. AFM images show NPL thicknesses to be 5 nm, in good agreement with the thickness of primary plates, capped with organic ligands. It is of note that some HRTEM images of the sheets show clear boundaries between the attached primary plates (SI Figure S10). We hypothesize that under ligand destabilizing conditions the NPLs assemble through oriented attachment into large thin sheets.

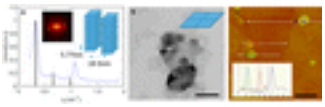

Figure 4. (a) Small angle X-ray scattering (SAXS) intensity map of dried NPLs sample. (inset) The anisotropic scattering intensity pattern is characteristic to oriented sheets. (b) Angular data yield peaks at q values of 1.068 and 0.327 nm^{-1}, corresponding to distances of 5.77 and 19.5 nm, the distance between centers of stacked NPLs and columns, respectively. Higher order peaks at 2q and 3q are also visible (black bars). (b) Two-dimensional sheets formed by lateral-oriented attachment of the primary (scale-bar 100 nm). (c) AFM topography micrograph depicting the $CsPbBr_3$ sheets with thickness ~5 nm (inset), while the lateral dimensions are on the order of 100 nm (scale bar is 500 nm).

In summary, the synthesis of highly luminescent (PLQY 84%), colloidal, $CsPbX_3$ NPLs was reported. NPLs with thickness of only a few integer number of perovskite unit cells (1–5), present clear quantum size effects. We demonstrated emissions covering the entire visible spectrum and self-assembly of NPLs into higher order hierarchies. Various optoelectronic application using perovskite NPLs with the already reported properties may be envisioned. However, further understanding and control over their surface chemistry and solution processability is essential for achieving those aspirations. Future studies of the perovskite NPLs will concentrate on these aspects.

Supporting Information

The Supporting Information is available free of charge on the ACS Publications website at DOI: 10.1021/jacs.5b11199.

- Experimental details, TEM, XRD, PL, and AFM data (PDF)

The authors declare no competing financial interest.

Acknowledgment

This work is supported by the Physical Chemistry of Inorganic Nanostructures Program, KC3103, Office of Basic Energy Sciences of the United States Department of Energy, under Contract No. DE-AC02-05CH11231.

- Reference QuickView

References

This article references 13 other publications.

1. (a) Schliehe, C.; Juarez, B. H.; Pelletier, M.; Jander, S.; Greshnykh, D.; Nagel, M.; Meyer, A.; Foerster, S.; Kornowski, A.; Klinke, C.; Weller, H. *Science* **2010**, 329 (5991) 550, DOI: 10.1126/science.1188035 [CrossRef], [PubMed], [CAS](b) Ithurria, S.; Tessier, M. D.; Mahler, B.; Lobo, R. P. S. M.; Dubertret, B.; Efros, A. L. *Nat. Mater.* **2011**, 10 (12) 936, DOI: 10.1038/nmat3145 [CrossRef], [PubMed], [CAS](c) Rowland, C. E.; Fedin, I.; Zhang, H.; Gray, S. K.; Govorov, A. O.; Talapin, D. V.; Schaller, R. D. *Nat. Mater.* **2015**, 14 (5) 484, DOI: 10.1038/nmat4231 [CrossRef], [PubMed], [CAS]
2. (a) Tang, Z.; Zhang, Z.; Wang, Y.; Glotzer, S. C.; Kotov, N. A. *Science* **2006**, 314 (5797) 274, DOI: 10.1126/science.1128045 [CrossRef], [PubMed], [CAS](b) Abécassis, B.; Tessier, M. D.; Davidson, P.; Dubertret, B. *Nano Lett.* **2014**, 14 (2) 710, DOI: 10.1021/nl4039746 [ACS Full Text], [PubMed], [CAS]
3. (a) Lee, M. M.; Teuscher, J.; Miyasaka, T.; Murakami, T. N.; Snaith, H. J. *Science* **2012**, 338 (6107) 643, DOI: 10.1126/science.1228604 [CrossRef], [PubMed], [CAS](b) Tan, Z.-K.; Moghaddam, R. S.; Lai, M. L.; Docampo, P.; Higler, R.; Deschler, F.; Price, M.; Sadhanala, A.; Pazos, L. M.; Credgington, D.; Hanusch, F.; Bein, T.; Snaith, H. J.; Friend, R. H. *Nat. Nanotechnol.* **2014**, 9 (9) 687, DOI: 10.1038/nnano.2014.149 [CrossRef], [PubMed], [CAS]
4. (a) Tyagi, P.; Arveson, S. M.; Tisdale, W. A. *J. Phys. Chem. Lett.* **2015**, 6 (10) 1911– 1916, DOI: 10.1021/acs.jpclett.5b00664 [ACS Full Text], [PubMed], [CAS](b) Sichert, J. A.; Tong, Y.; Mutz, N.; Vollmer, M.; Fischer, S.; Milowska, K. Z.; García Cortadella, R.; Nickel, B.; Cardenas-Daw, C.; Stolarczyk, J. K.; Urban, A. S.; Feldmann, J. *Nano Lett.* **2015**, 15 (10) 6521, DOI: 10.1021/acs.nanolett.5b02985 [ACS Full Text], [PubMed], [CAS](c) Dou, L.; Wong, A. B.; Yu, Y.; Lai, M.; Kornienko, N.; Eaton, S. W.; Fu, A.; Bischak, C. G.; Ma, J.; Ding, T.; Ginsberg, N. S.; Wang, L.-W.; Alivisatos, A. P.; Yang, P. *Science* **2015**, 349 (6255) 1518, DOI:

10.1126/science.aac7660 [CrossRef], [PubMed], [CAS]
5. Kulbak, M.; Cahen, D.; Hodes, G. *J. Phys. Chem. Lett.* **2015**, 6 (13) 2452– 2456, DOI: 10.1021/acs.jpclett.5b00968 [ACS Full Text], [PubMed], [CAS]
6. (a) Protesescu, L.; Yakunin, S.; Bodnarchuk, M. I.; Krieg, F.; Caputo, R.; Hendon, C. H.; Yang, R. X.; Walsh, A.; Kovalenko, M. V. *Nano Lett.* **2015**, 15 (6) 3692, DOI: 10.1021/nl5048779 [ACS Full Text], [PubMed], [CAS](b) Park, Y.-S.; Guo, S.; Makarov, N.; Klimov, V. I. *ACS Nano* **2015**, 9 (10) 10386, DOI: 10.1021/acsnano.5b04584 [ACS Full Text], [PubMed], [CAS](c) Swarnkar, A.; Chulliyil, R.; Ravi, V. K.; Irfanullah, M.; Chowdhury, A.; Nag, A. *Angew. Chem., Int. Ed.* **2015**, 276, DOI: 10.1002/anie.201508276 [CrossRef], [PubMed]
7. Son, J. S.; Wen, X. D.; Joo, J.; Chae, J.; Baek, S.; Park, K.; Kim, J. H.; An, K.; Yu, J. H.; Kwon, S. G.; Choi, S. H.; Wang, Z.; Kim, Y. W.; Kuk, Y.; Hoffmann, R.; Hyeon, T. *Angew. Chem., Int. Ed.* **2009**, 48 (37) 6861, DOI: 10.1002/anie.200902791 [CrossRef], [PubMed], [CAS]
8. Zhang, D.; Eaton, S. W.; Yu, Y.; Dou, L.; Yang, P. *J. Am. Chem. Soc.* **2015**, 137 (29) 9230– 9233, DOI: 10.1021/jacs.5b05404 ACS Full Text , [PubMed], [CAS]
9. Sadek, P. C. *HPLC Solvent Guide*; John Wiley and Sons, Inc., **2002**.
10. Grätzel, M. *Nat. Mater.* **2014**, 13 (9) 838, DOI: 10.1038/nmat4065 [CrossRef], [PubMed], [CAS]
11. Stoumpos, C. C.; Malliakas, C. D.; Peters, J. A.; Liu, Z.; Sebastian, M.; Im, J.; Chasapis, T. C.; Wibowo, A. C.; Chung, D. Y.; Freeman, A. J.; Wessels, B. W.; Kanatzidis, M. G. *Cryst. Growth Des.* **2013**, 13 (7) 2722, DOI: 10.1021/cg400645t [ACS Full Text], [CAS]
12. Tessier, M. D.; Mahler, B.; Nadal, B.; Heuclin, H.; Pedetti, S.; Dubertret, B. *Nano Lett.* **2013**, 13 (7) 3321, DOI: 10.1021/nl401538n [ACS Full Text], [PubMed], [CAS]
13. (a) Nedelcu, G.; Protesescu, L.; Yakunin, S.; Bodnarchuk, M. I.; Grotevent, M.; Kovalenko, M. V. *Nano Lett.* **2015**, 15 (8) 5635, DOI: 10.1021/acs.nanolett.5b02404 [ACS Full Text], [PubMed], [CAS](b) Akkerman, Q. A.; D'Innocenzo, V.; Accornero, S.; Scarpellini, A.; Petrozza, A.; Prato, M.; Manna, L. *J. Am. Chem. Soc.*

2015, 137 (32) 10276, DOI: 10.1021/jacs.5b05602 ACS Full Text, [PubMed], [CAS]

DISCLAIMER